Recent (2018–2021) glaciological, hydrological and geomorphological landscape changes of Hailuogou Glacier tongue, southeastern Tibetan Plateau

Shuyang Xu, Ping Fu, Duncan Quincey, Meili Feng, Stuart Marsh & Tian Jia

View supplementary material

Published online: 16 Dec 2022.

Submit your article to this journal

View related articles

View Crossmark data

Taylor & Francis
Taylor & Francis Group

Recent (2018–2021) glaciological, hydrological and geomorphological landscape changes of Hailuogou Glacier tongue, southeastern Tibetan Plateau

Shuyang Xu[a], Ping Fu[a], Duncan Quincey[b], Meili Feng[a], Stuart Marsh[c] and Tian Jia[a]

[a]School of Geographical Sciences and Geospatial and Geohazards Research Group, Faculty of Science and Engineering, University of Nottingham Ningbo China, Ningbo, People's Republic of China; [b]School of Geography and water@leeds, University of Leeds, West Yorkshire, UK; [c]Faculty of Engineering, Nottingham Geospatial Institute, University of Nottingham, Nottingham NG7 2TU, UK

ABSTRACT

Glaciers in the Tibetan Plateau are melting at an unprecedented recently rate in the context of global warming. Time-sequenced landform mapping for the Hailuogou Glacier, a partly debris-covered glacier in the southeastern Tibetan Plateau, shows the detailed evolution of glacier changes as the ice recedes. This study presents four maps of the Hailuogou Glacier tongue, a partly debris-covered glacier in the southeastern Tibetan Plateau, documenting the spatial evolution of glaciological, hydrological, and geomorphological features from 2018 to 2021. Structure from Motion with Multiview Stereo software was applied to images captured by from uncrewed aerial vehicles were used to produce digital surface models and orthophoto mosaics. These datasets were used, and then to identify and map the features based on pre-defined mapping criteria. From 2018 to 2021, the glacier underwent continuous recession, with the terminus retreating, intense crevassing in the lower part of the ablation zone, and continuous expansion of the terminal disintegration area. The recent evolution of the glacier implies that the gradual disintegration of the lower glacier tongue is likely to be exacerbated over the next decades by the continuous climate warming.

1. Introduction

Mountain glaciers all over the world have been receding at an unprecedented rate during the last decade (2010–2020) interpreted by the satellite and in-situ observations (Zemp et al., 2015), and they will continue to lose mass for further decades with predicted climate warming (IPCC, 2021). Many studies associated with mountain glacier changes have reported a substantial shrinkage of the glaciers in the southeastern Tibetan Plateau since the 1980s (Li et al., 2010; Liu et al., 2010). The sustained ice loss of glaciers in southeastern Tibetan Plateau has a clear impact on regional water supply and eco-environmental systems (Jouberton et al., 2022; Yang et al., 2013).

Persistently accelerated glacier mass loss may induce rapid changes in glacier dynamics, such that stresses and strain within the glaciers are redistributed in response to the mass perturbations, which then further alters the glacier structure (Azzoni et al., 2017). Rapid evolution in glacier dynamics forms a series of distinctive features on the glacier surface, and in the proglacial zones (e.g. crevasses, ice cliffs, proglacial rivers and vegetations). The analysis of the formation and development of these features can provide insights for improving the short- and long-term

projection of glacier evolution in the context of global climate change (Benn et al., 2017).

Hailuogou Glacier is a rapidly retreating temperate valley glacier in southeastern Tibetan Plateau with a disintegrating terminus. Several studies have investigated the recent changes of Hailuogou Glacier from the perspective of changes in the glacier geometry, glacier ice temperature, mass balance and glacial hydrology (Li et al., 2010; Liao et al., 2020; Liu et al., 2010; Zhang et al., 2010, 2011; Zhong et al., 2022). However, there are few detailed studies that characterize the evolution of the surface features. In this study, we provide detailed mapping results for the Hailuogou Glacier tongue using uncrewed aerial vehicle (UAV) photogrammetry. The aims are to (1) map the glaciological, hydrological and geomorphological features of the lower part of the Hailuogou Glacier valley (i.e. lower part of the glacier tongue, proglacial/paraglacial zones) through the high-resolution ortho-mosaics derived from UAV images collected in 2018, 2019, 2020 and 2021; and (2) discuss the spatiotemporal evolutions of the Hailuogou Glacier from 2018 to 2021 based on the changes in particular features (e.g. ice crevasses and ice cliffs).

2. Study Area

Hailuogou Glacier (Figure 1) is a partly debris-covered temperate glacier in the southeastern Tibetan Plateau (Liu et al., 2010). It is an east-flowing glacier originating from the summit of Mt. Gongga (7556 m a.s.l.) with a length of ca.11.97 km and an area of ca. 24.7 km² in 2021 (Wang et al., 2021; Zhong et al., 2022). The glacier has a steep icefall with an elevation difference of ca. 1080 m (Figure 2(A)), connecting the
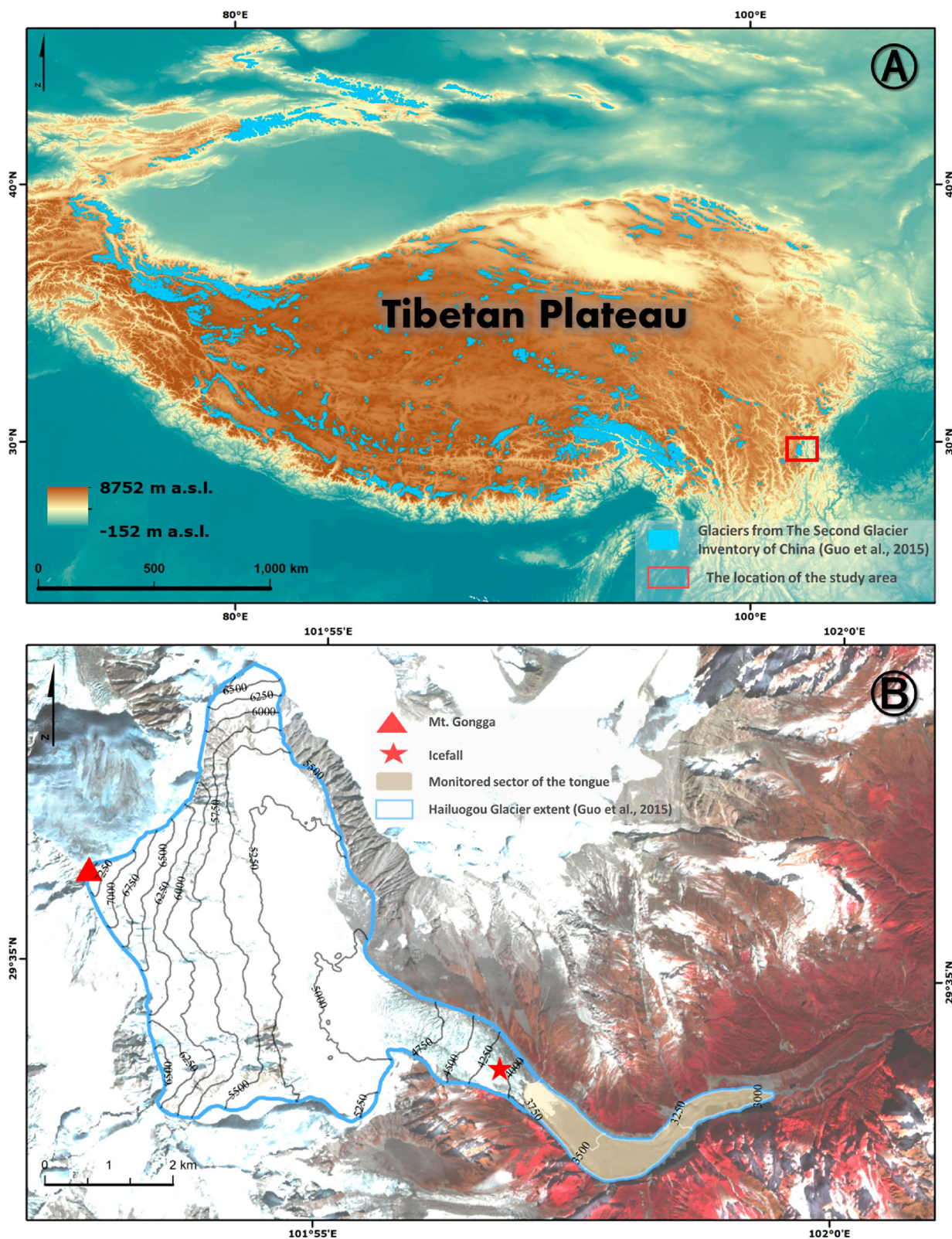
Figure 1. A: The study area is located in the southeastern Tibetan Plateau and the distribution of glaciers of Tibetan Plateau. The elevation data is extracted from GTOPO30 (USGS, 1997) B: The Hailuogou Glacier, southeastern Tibetan Plateau and the monitored sector of the glacier tongue. The background image is the false color composite of Sentinel 2A on the 10ᵗʰ November 2020. The Hailuogou Glacier outline and the distribution of glaciers in the Tibetan Plateau is from the Second Glacier Inventory Dataset of China version 1 (Guo et al., 2015).

Figure 2. A: The icefall with elevation differences of ∼1080 m (image date: July 2021). Areas marked with red boxes are the exposed bedrocks due to the intense ablations. B: The viewing in the middle section of the glacier (∼3250 m a.s.l.). The glacier surface is covered by debris-mantle and intensively crevassed (image date: July 2021). C: The scene from the old viewing platform (∼ 3180 m a.s.l.). The glacier surface is highly debris-covered. Several long ice cliffs were exposed, and a highly crevassed lateral margin induced by external stream can be seen (image date: July 2021). D: The highly crevassed glacier terminus with frontal ice collapsing, and the proglacial river flows from the subglacial channel outlet (image date: July 2021). Blue arrows indicate the external streams flow into the glacier lateral margin from higher elevation (e.g. fed by tributary small glaciers).

firn basin (4980–7556 m a.s.l.) and the lower glacier tongue (2900–3900 m a.s.l.) (Li et al., 2010).

Due to rapid ablation being experienced across the glacier tongue, coupled with a reduction in ice flux from the up-glacier accumulation zone, the icefall has thinned and narrowed, and bedrock has become increasingly exposed since the appearance of the first glacier-hole at the icefall in 1993 (Li et al., 2010). The bottom of the icefall (i.e. the upper section of the glacier tongue) has a gradient of ∼10° and is partly covered by an fan-shaped structure formed by ice avalanching from the icefall (Zhong et al., 2022). The part below the icefall is about 5 km in length and 300-500 m in width, and is overlain by supraglacial debris (i.e. the thickness of debris-covers varies from several millimeters below the icefall to more than 1 m at the glacier terminus area) due to the processes of frost weathering and rock avalanches (Zhang et al., 2011, 2012). Glacier flow gradually transitions from southeast-orientated to northeast-orientated, forming a glacier arch with intense crevassing in the middle part of the glacier tongue. Several seasonal streams flow from

higher cliffs into the hydrological system of the glacier, draining out from the subglacial channel outlet in the highly crevassed terminus (Figure 2).

Previous works have addressed the rapid changes in the Hailuogou Glacier, in terms of changes in the surface geomorphology, glaciological landscapes, glacier mass balance and the glacial hydrological system (e.g. Heim, 1936; Huang et al., 1996; Liu et al., 2010; Liu & Liu, 2010; Lu & Gao, 1992; Zhang et al., 2012). Accelerated warming since the 1980s has exerted profound effects on glacier dynamics. Recent studies have demonstrated that the Hailuogou Glacier underwent severe recessions, particularly in terms of ice collapse events at the glacier terminus (Xu et al., 2022; Zhong et al., 2022).

3. Data and Methods

3.1. Data sources

3.1.1. UAV and flight mission
Four field trips to Hailuogou Glacier were conducted during the ablation seasons from 2018 to 2021 (S-
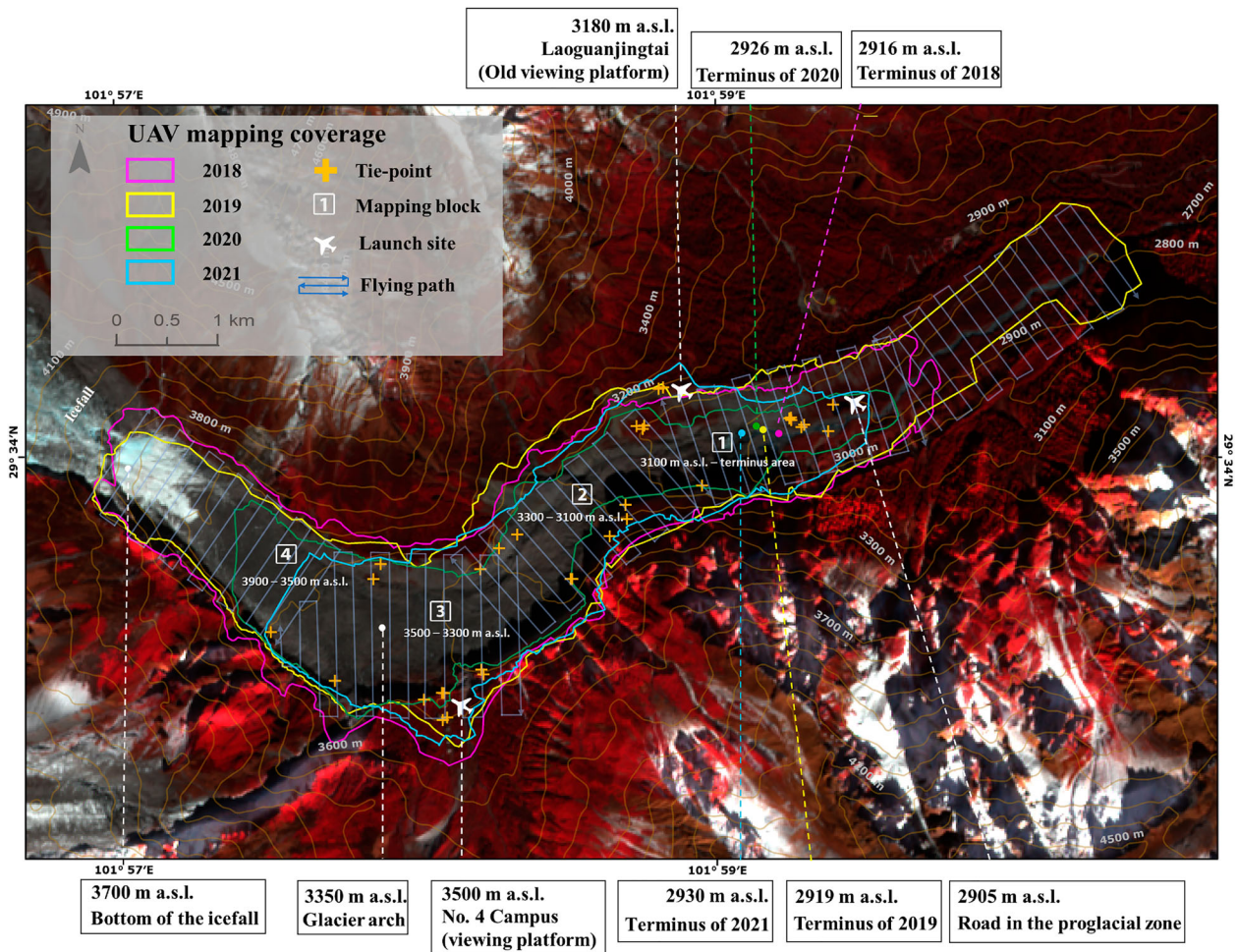
Figure 3. The spatial coverage of four UAV mapping areas and their elevation ranges, the distribution of the tie-points, the flight pathways, and the locations of three launch sites. The background image is the same as in Figure 1.

Table 1). The first three surveys (June 2018, October 2019 and September 2020) used a DJI Mavic Pro (12.71 megapixels for the camera sensor), and the fourth survey (July 2021) used a DJI Mavic Pro 2 Enterprise Advanced (48 megapixels for the camera sensor).

Flight missions differed with launch sites and flying heights as the surface elevation of the glacier tongue ranged from 2920 m a.s.l. (i.e. the glacier terminus of 2021) to 3900 m a.s.l. (i.e. the bottom of the glacier icefall) with consistent ground sample resolution. The glacier tongue was mapped separately with four gridded blocks and the UAV was launched from three sites as shown in Figure 3. The onboard camera was maintained in a nadir viewing angle for ortho-photogrammetric mapping with a lateral overlap and longitudinal overlap of 70% and 80%, respectively. The flight missions were pre-programmed and conducted in automatic mode. Each UAV survey has a total length of 60 km flight path, taking around 1.5 hours in flight duration to cover the entire glacier tongue in each case. The mapping area was divided into four gridded flight paths and covered separately with variable flying elevation in order to keep constant ground sample resolutions. Specifically, the glacier tongue was divided into four elevation bands for UAV mapping and further analysis of feature changes: < 3100

m.a.s.l (Sector 1), 3100–3300 m.a.s.l (Sector 2), 3300 - 3500 m.a.s.l (Sector 3), > 3500 m.a.s.l (Sector 4) (Figure 3). Nearly 8900 images were acquired in the four flight missions. Additional images captured by manual operation were needed depending on the unsteady weather and lighting conditions in the glacier valley.

3.1.2. Tie points
Limited by the scale and the rugged surface of the glacier tongue, it is impractical to set ground control points byduring UAV missions. The primary embedded GNSS sensors of the UAV enable meterscale accuracy in location. For the most recent (2021) survey, we benefited from an external realtime kinematic plug-in, and therefore achieving high accuracy photogrammetric mapping without external ground control points from GNSS equipment. The real-time kinematic plug-in records the coordinates with a mean root mean square error of 1 cm + 1 ppm (i.e. 1 ppm means the error has a 1 mm increase for every 1 km of movement from the drone) horizontally and 1.5 cm + 1 ppm vertically (Zhong et al., 2022). Accordingly, we considered the most recent dataset as the benchmark and extracted 33 points
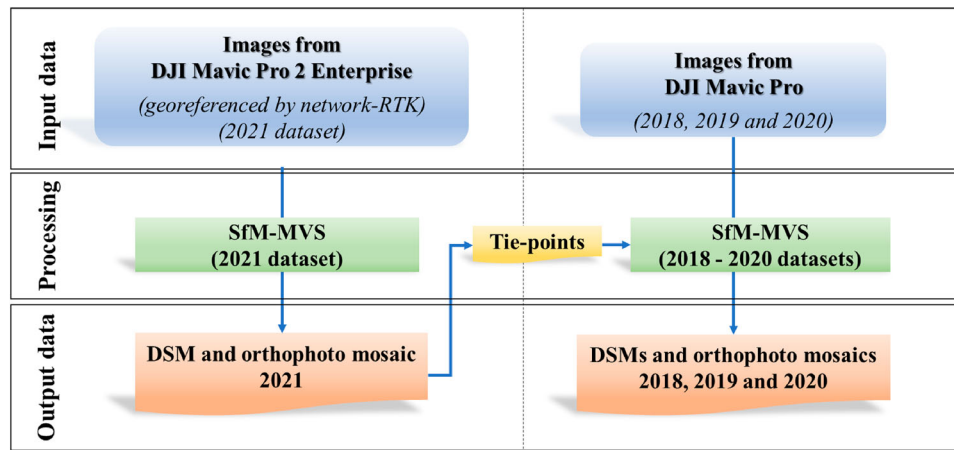
Figure 4. Workflow of UAV image processing was applied to datasets of 2018, 2019, 2020 and 2021 to derive the DSMs and ortho-photo mosaics. Tie-points were extracted from the datasets of 2021 and then used for co-registering with 2018, 2019 and 2020 datasets.

that are easily identifiable and stable surface features from it as the tie-points (Figure 3).

3.2. Methods for map production

3.2.1. Digital surface models (DSMs) and orthophoto mosaics

Multitemporal ortho-mosaics and digital surface models (DSMs) were produced based on Structure from Motion with Multi-View Stereo (hereon, SfM-MVS) in Agisoft Metashape Pro v1.5.3 (Agisoft LLC, 2020). We followed the standard SfM-MVS workflow (Figure 4) as illustrated by other papers in detail (e.g. Bash et al., 2018; Chudley et al., 2019; Mallalieu et al., 2017; Rossini et al., 2018; Smith et al., 2016). Tie-points were extracted from the 2021 dataset for co-registration with the earlier three datasets (i.e. all root mean square errors < 0.94 m; refers to S-Table.1).

3.2.2. Features mapping

Identification and mapping of the landform features depend on the premise that the landform features have distinctive traits that can be used to extract and categorize them (Chandler et al., 2018; Fu et al., 2013). A variety of factors affect how the criteria of feature identification and extraction are defined, including means of data acquisition, the methodology of mapping, and the life cycle of targeted features.

From the DSMs and ortho-mosaics, the primary features were visually interpreted and manually mapped within ArcGIS 10.3 (Figure 5). To ensure the precise interpretation of the features, the three-dimensional scene of the dense point clouds and DSMs were consulted in cases of ambiguity, such as where the boundary between marginal ice cliffs and the valley walls was unclear, or where the orientation of ice cliffs was vertically variable. The use of multiple viewing perspectives in this way is important because three-dimensional viewing can provide information

on the structure and morphology of the features, which is not always immediately apparent from the two-dimensional perspective.

4. Mapped feature and identification criteria

The evolution and spatial distribution of features in the glacier valley result from the varying controls on glacier motion, glacier hydrology, erosion, deposition, surrounding topography and ice thermal regime. Representative features need to be predefined to characterize the changes in the glacier valley. To achieve this, we classified the features into four categories: (i) Glaciological features related to structural deformation of glacier ice and surface motion; (ii) hydrological features associated with the transport of meltwater and external water; (iii) geomorphological features in relation to effects of past glaciations; (iv) other landforms in the valley.

4.1. Glaciological features

4.1.1. Crevasses

Crevasses are open cracks in the glacier ice formed by changing stress as the glacier flows (Colgan et al., 2016; Jennings et al., 2016). The spatial distribution of crevasses provides information on the adjustment of stress and strain within the glacier (Goodsell et al., 2005; Jones et al., 2018). Once the stress exceeds the critical threshold (i.e. the strength of ice body), the ice fractures to form ice crevasses with different widths, lengths, and orientations, marking significant evidence of glacier changes (Benn & Evans, 2013; Vaughan, 1993).

Crevasses dominate the Hailuogou Glacier tongue. Crevasse lengths range from less than a meter to more than 130 m, and the widths are consistently less than 10 m. We identified them by the generally curved dark cracks and mapped as polylines. Although
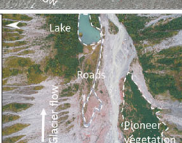
		Landforms	Example	Description	Interpretation	References
Glaciological landforms	A	Crevasses		Curved-shaped open dark cracks on the glacier surface. This is a ubiquitous feature across the glacier surface. Four main types on the Hailuogou Glacier: splaying crevasse, en-echelon crevasse, transverse crevasse and longitudinal crevasse (Jennings and Hambery, 2021).	The representative of the brittleness in the glacier dynamics and it is formed from the internal stress exceeding the ice strength. The pattern of crevasses varies depending on the internal force field. Mapped as polylines.	Colgan et al., (2016) Jennings et al., (2016) Jennings and Hambrey, (2021) Jones et al., (2018) Goodsell et al., (2005) Benn and Evans, (2013)
	B	Ice cliffs		Zonal bare (or thin debris-covered) glacier ice with crescent-shaped, semicircular-shaped, circular-shaped, half arch-shaped or linear banded structures.	Ice cliffs create spots with higher ablation rate than the surrounding debris-covered ice surface. They are usually formed by the depression of the ice surface induced by conduit's roof reduction, or the ice strength, or the surface being exposed due to the deep slope and the glacier dynamics. Mapped as polygons	Watson et al., (2017) Sakai et al., (2002) Kirkbride and Warren, (1999) Kirkbride et al., (1993) Kneib et al., (2021)
	C	Inter-crevasse blocks		A patch of highly crevassed glacier surface, mainly affected by the external water supply from lateral higher elevation. The crevasses are centered at the inlet of the external runoff and organized in a radial pattern. The closer to the margin of the glacier, the more it is fragmented.	This set of crevasses is formed by the impacts of perennial runoff (fed by tributary glaciers within the valley). As a combined result of intense ablation and the external water, a highly and radially crevassed surface can be developed in the lower and middle parts of the tongues (i.e., thinned ice body). Mapped as polygons	Jennings and Hambrey, (2021)
	D	Features associated with icefall		Fresh ice can be identified by pure white color and the avalanche traced can be consequently derived. The exterior fan-shaped structure is induced by ice avalanches and melting. The thinly-debris covered ice surface is below the fan structure. The color is progressive transition from pure white to gray-black.	The three fan-shaped features associated with ice debris avalanched from icefall show a progressive transition from icefall bottom to upper part of the ice tongue. Mapped as polygons	Su et al., (1996) Zhang et al., (2010)
Hydrological landforms	E	Supraglacial pond		Milky-coloured features, often approaching a circular shape, and surrounded by glacier surface debris	The major component of water storage on the glacier surface generally formed at depression area fed by the meltwater from the glacier surface drainage system or local melting. Mapped as polygons	Watson et al., 2016 Yang and Liu, (2016) Lardeux et al., (2021) Miles et al., (2017)
	F	Stream		The alternative surface surface streams from the melting of upstream ice and higher elevation. The stream flows into the glacier from an inlet at the glacier lateral margins.	Perennial runoff (i.e., fey by small hanging glaciers in the HLG basin) and non-perennial runoff (irregular periodic runoff flowing from the conifer forest at the top of the valley cliff) coexisted in the valley. Mapped as polylines	Liu and Liu, (2010)
	G	Proglacial waterbody		Proglacial pond and proglacial river. Proglacial rivers are usually muddy with a milky or earthy color as they contain substantial volumes of glacial sediments. Proglacial ponds are relatively small and approaching a circular shape. The colors are clear and earthy-colored, probably due to their different formation mechanisms.	HLG Glacier has a perennial proglacial river discharging water from its hydrological system and it carries glacial deposits from the glacier erosion. Some clear proglacial pond may be kettles as the melted out of the isolated dead ice blocks. Some earthy-colored pond may be left by the variation of braided river.	Jones et al., (2018)
Geomorphological landforms	H	Lateral moraine		Lateral moraine of HLG Glacier is distinctive from its terminal moraine as some of them are well preserved. Ridge-shaped marginal features, commonly found along the glacier sides and consist of debris from the slope failure or the accumulation of paleoglacier surface.	The forest of *Abies fabri* can be found at the top of both of the lateral moraines, which is stable since Little Ice Age (Zhong et al., 2022). The height of lateral moraines to the present glacier surface ranges from ~80 to 160 m. A cableway connects the lateral moraines on it north and south sides. Mapped as polygons	Zhong et al., (2022) Benn and Evans, (2013) Fu et al, (2012)
	I	Glacial polished rock wall		Faceted features, often found at the lateral side of the valley wall, with grooves and scratches of varying depth on the surface. Some of them are partly covered with vegetation.	The basin walls were progressively polished by the erosion of the glacier, and they left scrapes as traces of former glacier in eroding the walls, a trail of the dynamics of the paleo-glaciers. Mapped as polygons.	Darnault et al., (2012) Owen et al., (2008)
	J	Trimline		Linear feature along the sidewalls of the valley. A series of edges delineating the well-vegetated from poorly vegetated regions.	Denotes a former maximum extent of the glacier. Mapped as polylines.	Li and Fu, (2019)
Other	K	Artificial lake, roads, and vegetations		An artificial lake and roads located in the proglacial area. And pioneer vegetations occupied the proglacial zone and both of lateral sides of valley walls (i.e., herbaceous species). Abies fabri forests are steadily occupied the ridge sides of lateral moraines since LIA	Mapped as polygons	Zhong et al., (2022)

Figure 5. Visual identification of features in the Hailuogou Glacier valley.

crevasses have different widths and depths, we only mapped them along their long axes (Figure 5(A)). Their morphology changes along with the glacier longitude profile. For instance, crevasses in the upper section of the glacier tongue appear as relatively long and splaying, aligned with low spatial density. The uppermost crevasses were orientated parallel with the direction of glacier flow. Conversely, in the middle section of the glacier tongue, the orientation of the crevasses was transverse to the direction of the glacier flow. In the lateral margin of the glacier, the crevassed surface may be formed by rotational strain within the ice along the edges. The morphology of ice crevassing is affected by the existence of water to

some extent (Sakai et al., 2009), particularly for the regions of the inlets of streams from the higher elevation of the valley walls. The ice here becomes more fractured, resulting in more crevassed areas surrounding the inlets.

4.1.2. Ice cliffs

Ice cliffs are commonly described as (sub-) vertical ice walls, usually found around the margins of supraglacial ponds (Watson et al., 2017). For debris-covered glaciers, ice cliffs may be formed in two processes (Kirkbride, 1993; Kirkbride & Warren, 1999; Sakai et al., 2002), specifically, the first process is resulted from the sliding of supraglacial debris due to a steepening slope; the second is associated with surface depressions caused by roof collapse of a subglacial or englacial channel.

Here, we delineate ice cliffs as exposed ice faces with either clean ice or dirty ice (i.e. slightly thin debris on the surface) (Watson et al., 2017) (Figure 5(B)). Ice cliffs are apparent and the majority of them are observed as linear banded, crescent-shaped, and half arch-shaped bare glacier ice surrounded by relatively thin debris mantle. There are two patterns of ice cliffs on the Hailuogou Glacier tongue by the philosophy of ice cliff formation (Sakai et al., 2002). A large amount of linear banded and crescent-shaped ice cliffs was identified on the lower section of the glacier tongue. The ice cliffs in this region might be formed by the exposure of the subglacial channels or voids due to the intensified glacier surface lowering (Li et al., 2010). The remaining ice cliffs were distributed across the upper section and lateral sides of the glacier tongue; most of them were exposed by debris sliding as a consequence of a steepening surface or ice crevassing.

4.1.3. Inter-crevasse blocks

Inter-crevassed blocks (Figure 5(C)) refer to a cluster of highly fractured ice bodies where seracs develop between crevasses (Jennings & Hambrey, 2021). The inter-crevassed blocks of the Hailuogou Glacier are found at the north lateral margin (i.e. 3250 m a.s.l.). Here, there is a lateral stream flowing from the higher elevation into the lateral margin of the Hailuogou Glacier. The continuous effect of external water on the glacier ice gradually erodes the surface. The inter-crevassed blocks on Hailuogou Glacier were most likely formed by spatially variable glacier dynamics as well as the effects of frequent and persistent water activity.

4.1.4. Features associated with icefall

The icefall (i.e. 3650-4980 m a.s.l.) transports the ice mass down-valley, controlled by the rapid extrusion of ice flow and disorganized ice crevassing (Zhang et al., 2010). In the zone between the base of ice fall and the upper part of the middle section of the glacier tongue, which is also the transition zone of extending and compressional ice flow, there are particular features mainly associated with avalanches of the icefall, namely fresh ice, an ice fan and thinly debris-covered ice (Su et al., 1996) (Figure 5(D)).

These three features show a clear spatial pattern (see example in Figure 5(D)). Specifically, the uppermost portion is fresh ice, most of which is composed of ice chunks with a long axis of 1-2 m. Fresh ice can be identified by its white color, and the avalanche trace can be roughly identified consequently. Exterior to the fresh ice is a fan structure formed by successive avalanches (and subsequent melting) of ice. This fan-shaped structure is distributed in a tongue-like pattern, with a length of ~1000 m and a width that traverses the entire glacier. It is primarily composed of the varied size of firn and ice, with a mixture of ice and rock, yielding them gray and yellow-white in color. Below the fan-shaped structure is the ice surface with a thin debris cover, which can be considered as the transition zone between clean ice and the debris-covered surface.

4.2. Hydrological features

4.2.1. Supraglacial pond

Supraglacial ponds (Figure 5(E)) store the majority of meltwater on glacier surfaces. Ponds generally form in natural depressions and are fed by meltwater from the glacier surface drainage system or local melting (Watson et al., 2016; Yang & Liu, 2016). Ablation is highly spatially variable according to the varied thickness of the debris mantle. This difference in ablation between debris-covered ice and debris-free ice often creates an undulating topography with natural pits in which meltwater can collect (Lardeux et al., 2016). After the formation of supraglacial ponds, the meltwater stored by these ponds promote ablation to facilitate the edges becoming steeper, such that the debris cover thins, and ablation is further enhanced in a mechanism of positive feedback (Miles et al., 2017). Some supraglacial ponds might drain out following hydrofracture (Liu et al., 2018). Their life cycle is short due to the rapid thinning of the glacier tongue and frequent collapse of subglacial channels, so their existence may not persist between sequential surveys. The supraglacial ponds mainly distributed in the lower patch of the glacier tongue (i.e. areas lower than 3500 m a.s.l.), with some outward ice cliffs and some lateral crevasses.

4.2.2. Stream

The Hailuogou Glacier has a well-developed hydrological system in its lower ablation region (Liu & Liu, 2010). External waters from higher elevations flow into the drainage system within the glacier and discharge through the subglacial channel outlet along

with the meltwater, forming the proglacial river. The majority of streams (Figure 5(F)) on the study site were defined as the streamflow at the lateral side of the glacier valley from the higher elevation and some of them were additionally fed by the nearby small glaciers.

4.2.3. Proglacial waterbody

Proglacial waterbodies of the Hailuogou Glacier (Figure 5(G)) include the proglacial river and proglacial ponds. The proglacial river is not only the main force eroding the proglacial zone and periglacial zone, but also the sources of sediments. The proglacial zone is shaped by the evolution of the proglacial river, which forms highly active braided stream networks (Jones et al., 2018). Proglacial ponds usually occur near the south and north side of the proglacial river. They are commonly seen as single water features or a series of circular intersecting ponds.

4.3. Geomorphological features

4.3.1. Lateral moraine

Moraine is the accumulation of till material that is laid down by glaciers or ice shelves (Benn & Evans, 2013). Glacial till refers to all loose sediments produced, transported, and deposited by the glacier. Glacial till is ubiquitous across the glacier system, and it includes every size of glacial sediment, from silt-sized glacial flour to large boulders. They mound to form a ridge of unsorted sediments called the end moraine, and the farthest end moraine is the terminal moraine for a glaciation. Lateral moraines (Figure 5(H)) refer to ridge-shaped marginal features commonly found along the lateral sides of the glacier valley (Fu et al., 2012). For Hailuogou Glacier, the lateral moraine is distinctive, but it also needs to be carefully cross-compared with the orthophotos and DSMs to identify the glacier margin. The terminal moraine is absent, so, this area is therefore mapped as proglacial till.

4.3.2. Glacial polished rock wall

Polished rock walls (Figure 5(I)) are referred to as the glacial eroded lateral cliffs in the glacier valley. Polished rock walls in the Hailuogou Glacier valley can be found on both lateral cliffs. On these walls, various glacial erosion trails can be identified, such as striae, grooves and fissures. Over the study period, the polished rock walls were mapped with varying-sized polygons due to the vegetation cover on the walls.

4.3.3. Trimline

The trimline (Figure 5(J)) is an almost horizontal linear landform feature usually found along the sidewalls of a glacial valley. It marks the higher elevation of the erosion by the former glaciation and serves as an indicator of the thickness of the previous glacier (Li & Fu, 2019). During previous glaciations, the glacier advanced downstream and removed the vegetation on the surface by erosion. With the glacier retreating and the surface lowering, a series of distinct edges on the hillsides can be identified to separate the well-vegetated terrain from the poorly vegetated region (i.e. glacier-eroded area). Based on the sharp contrast of the color and textures on the slope, the trimlines in the Hailuogou Glacier valley are particularly clear. Some parts of the trim-line were interrupted by lateral landslides due to the unsteady paraglacial slope.

4.4. Other features

Three other features (Figure 5(K)) in the glacier valley were also mapped, categorized simply as artificial lake, road, and vegetation.

5. Results

The spatiotemporal changes of the mapped features were compared year by year. It should be noted that the two most recent maps (2020 and 2021) have limited data for Sector 4 (i.e. 3576 and 3521 m a.s.l. for their upmost elevation, respectively). Therefore, only three Sectors (1-3) were used for the 2021 datasets, and elevations ranging from 3500 to 3576 m a.s.l. were taken as the extent of section 4 for the 2020 dataset. To illustrate ice crevasse orientation and ice cliff aspect, the eight cardinal and intercardinal points of the compass were used (Figure 6 and S-Table 2). Areal and surface elevation data for the four sectors of the glacier are illustrated in Figure 7(A,B), respectively. The statistical analysis for crevasses, and ice cliffs, is summarized in Figure 6, Figure 7(C,D). Changes in supraglacial pond characteristics are listed in S-Table 5.

Hailuogou Glacier has been in rapid recession during the observation period, as demonstrated by the areal decline of the lower part of the glacier tongue (Figure 7(A) and S-Table-6). A decrease in surface elevation has been observed along the glacier center flowline (Figure 7(B)). Figure 7(B) demonstrates clearly that the glacier terminus retreated more than 300 m and the elevation of the terminus climbed from 2916 to 2930 m a.s.l. over the observation period.

5.1. 2018 surface features

On the 2018 map, ice crevasses mainly present a NE-SW orientation for Sectors1 and 2, while those in Sectors 3 and 4 are orientated NW-SE instead (refer to S-Table 2). Sector 4 has the highest crevasse density (i.e. 41.27 km/km^2), which was about twice as high as Sectors 2 and 3, and five-times higher than Sector 1 (see Figure 7(C)).
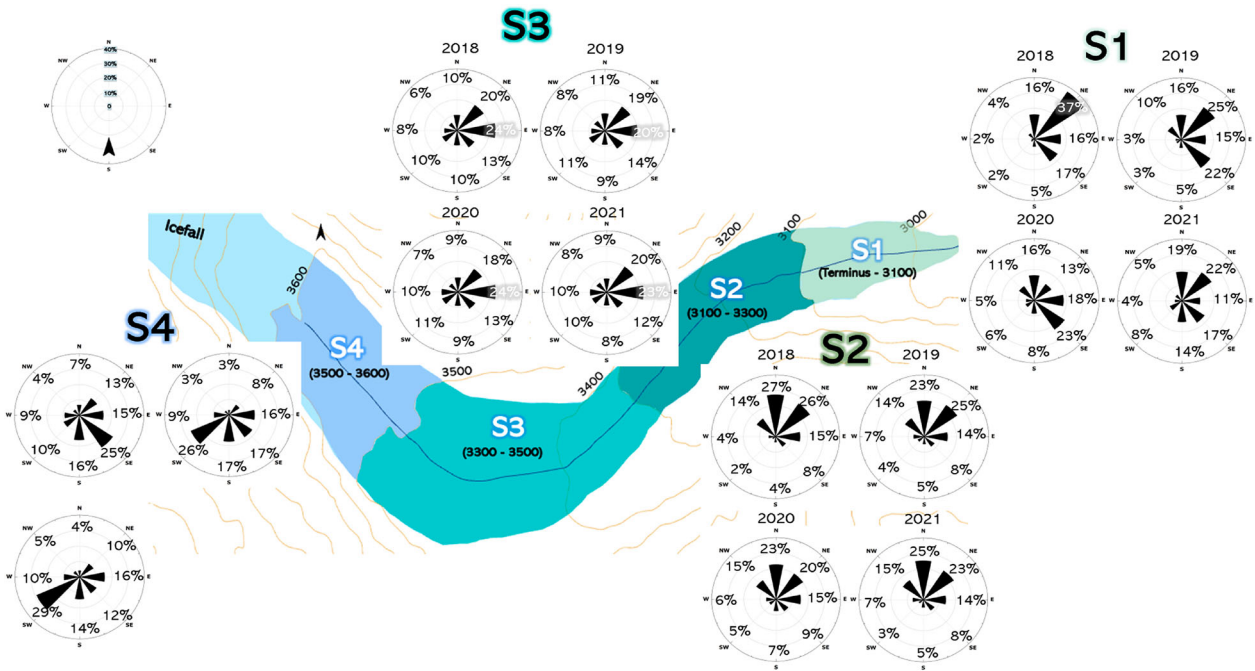
Figure 6. The ratio of each aspect (eight directions) of the ice cliffs in each sector. The center map shows the spatial distribution of the four elevation sectors. Please refer to S-Table 7 for detailed statistics of ice cliff orientations.

The density of ice cliffs reaches 17.74% in Sector 3, whereas ice cliff density in lower sectors do not exceed 13% (see Figure 7(D) and S-Table 3). NW and N are the dominant aspects for Sectors 1 and 2 (i.e. 36.96% and 27.21%; Figure 6 and S-Table 3), respectively, while W and SW are dominant in Sector 3 and 4
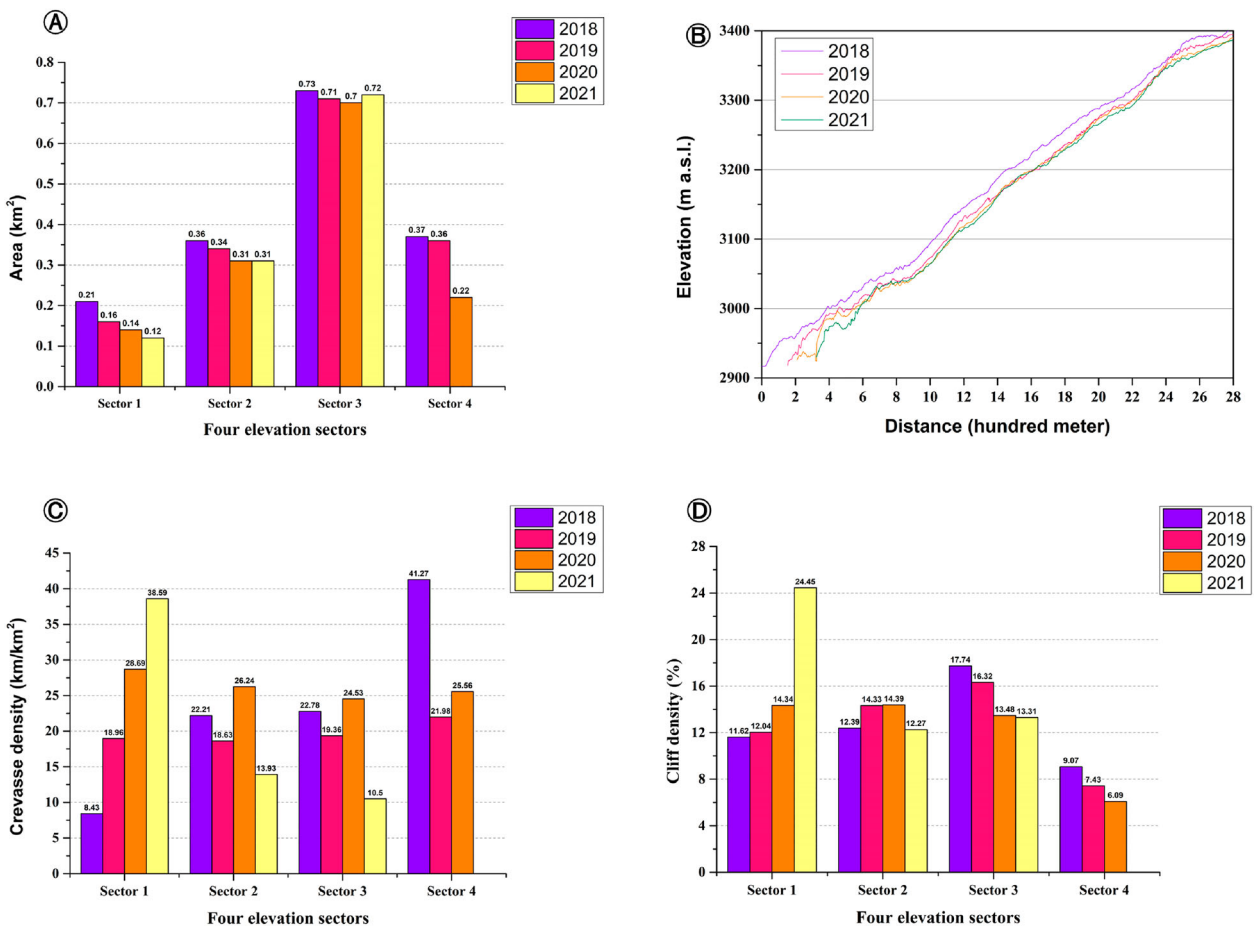

Figure 7. A: The annual area changes for each elevation sectors. B: Ice surface elevation along the glacier center flow line. C: Crevasse densities for four elevation sectors. D: Ice cliff densities for four elevation sectors.

respectively, with neither less than 23%. For the whole mapped region, NW and W are dominant in determining ice cliff orientation, adding up to more than 43% of the total.

5.2. 2019 surface features

Crevasse directions exhibited in 2019 were largely consistent with those mapped in 2018. However, the total length of the crevasses declined by more than 10 km during the intervening period (S-Table 4). Crevasse density in 2019 reached the highest value in Sector 4, similar to that evident in 2018 (21.98 km/km^2) (Figure 7(C)). The overall density of crevasses for the entire glacier tongue during 2019 was lower by about 5 km/km^2 compared to the previous year (S-Table 4). The density of cliffs this year retained a similar pattern as to the 2018 map (Figure 7(D)), that is, Sector 3 had a maximum density of around 16%, followed by Sectors 2, 1, and 4 (all in excess of 7%).

For ice cliff aspect, the primary orientation was NW- and W-facing, with a range from 20 to 26% of all cliffs in these categories for Sectors 1–3 (Figure 6 and S-Table 3). However, SE-facing cliffs occupied about 26% of the total for Sector 4, exceeding all other orientations. As per the 2018 map, the dominant orientation overall was NW and W, occupying around 20% of all cases (S-Table 3).

5.3. 2020 surface features

Here, elevations from the glacier terminus up to 3576 m a.s.l. were considered within Sector 4. The crevasse orientations of Sectors 1–3 are dominated by both NW-SE and NE-SE, and Sector 4 is also occupied primarily by NW-SE orientated crevasses (S-Table 1). Although the mapped region is less extensive than in 2019, the total length of mapped crevasses is about 35 km, more than 4 km longer than in 2019 (S-Table 4). Crevasse densities are largely consistent, ranging from 24.53 to 28.69 km/km^2 (Figure 7(C)). In contrast to the two previous maps, the highest density occurs in Sector 1, where the crevasses are concentrated at the glacier terminus and produce large ice cliffs.

According to Figure 6, cliff aspects of Sectors 1–3 are dominated by SW, N, and W-faced cliffs with about a ratio of 22%, while the minimum aspects are SE, E, and NE with a ratio of less than 6.53%. For Sector 4, the primary direction is similar to 2019 maps, that is SE. As a whole, the dominant orientation of 2020 is W (i.e. 20.65%) and NW (17.06%), whereas the fewest cliffs face NE and E.

5.4. 2021 surface features

As there are no data for Sector 4 in 2021, we concentrate here on Sectors 1–3. The primary direction of ice

crevasses is consistent with the 2020 map (S-Table 2). The total length of crevasses is 16.74 km, which is around 12, 7, and 10 km less than in 2020, 2019, and 2018, respectively (S-Table 4). The crevasse density of Sector 1 is high (38.59 km per square kilometer), which is comparable only to the value calculated for Sector 4 of 2018 (see Figure 7(C)). This illustrates the highly crevassed glacier surface near the glacier terminus. Further, the density of ice cliffs in section 1 is noticeably higher than in other sections, at around 24% (Figure 7(D)). The first and second primary directions for the ice cliffs are a combination of N and NW or NW and W. The cliffs with SE, E, and NE orientation are least common within the three sectors.

6. Discussion

6.1. Uncertainty analysis

6.1.1. Uncertainty from UAV-derived datasets

Acquiring high-quality aerial images in highly rugged mountainous regions (e.g. Hailuogou Glacier valley, southeastern Tibtetan Plateau) by UAV is challenging. The highly variable microclimate within the Hailuogou Glacier valley may induce rapid changes in regional weather, such as mist/fog and clouds, which further causes uneven lighting and unexpected shadows during conducting UAV surveys (Xu et al., 2022). However, visual checking of the sparse and dense point cloud shows that the images with severe shadows were not aligned and were not further processed, and therefore the impacts on the DSM and orthophotos are minimal.

The rigorous ground control points obtained from external GNSS equipment are necessary for conventional photogrammetry (Gindraux et al., 2017). The quality of the absolute georeferencing of the generated DSMs and orthophotos relies on the number of ground control points and their spatial distributions across the study area (Villanueva & Blanco, 2019). However, it is impractical to collect the coordinates of ground control points on the highly crevassed surface of the Hailuogou Glacier. Therefore, our approach is utilizing the orthophoto of July 2021 as the benchmark (i.e. georeferenced by network-RTK) and then co-align the remaining three surveys to this benchmark with 33 tie-points extracted from the 2021 orthophoto (Forlani et al., 2018). Based on that, four DSMs with a spatial resolution of no more than 0.36 m/pixel and orthophotos with a spatial resolution of no more than 0.09 m/pixel were produced from the SfM-MVS workflow (refer to S-Table 1). The final root mean square errors from co-aligning with the benchmark dataset are all less than 0.94 m. Although some minor errors might occur in relation to the setting of tie-points for each dataset

(2018, 2019, and 2020), their impacts are assumed minimal.

6.1.2. Uncertainty from mapping results

Due to the fact that all mapping works were done manually, it is not possible to calculate the range of uncertainty, therefore, we mainly focus on the sources of uncertainty in the mapping work. The arguments are mainly from two aspects: (1) the changes in the density of ice crevasses, and (2) the statistics of the area of each glacier sector (i.e. the delineation of glacier margins).

It can be referred from the Main maps A and B that there is a clear reduction in crevasse density, which can also be interpreted by comparing the orthophoto between 2018 and 2019 (S-Figure 1). As stated in the mapping criteria, we mapped the long axis of the crevasses with polylines, which means we only mapped the length of the crevasses, but the width is ignored. However, the width of crevasses in 2018-Sector 4 is much less than that in 2019-Sector 4. In the context of continued glacier ablation, although the ice crevasse density decreased significantly in 2019 (when counting crevasses length only), the reason for the decrease may be attributed to the fact that the width of ice crevasses is gradually becoming larger. In other words, many long and slender ice crevasses are integrated into massive crevasses with wider widths due to deepening and intense ablation.

The reliability of calculating the change in glacier area can be interpreted as the reliability of outlining glacier margins. It is difficult to distinguish the lateral margin of the glacier, even with very careful cross-referencing of orthophotos, DSM, and 3D point clouds, For instance, the middle part of the Hailuogou Glacier tongue (i.e. Sector 3) is covered by thick debris cover, especially for the lateral margins (S-Figure 2) (Zhang et al., 2019). Therefore, it may bring slight errors when outlining the glacier lateral edge of Sector 3. For Sectors 1, 2 and 3, lateral crevasses or some vegetation can indicate the possible lateral glacier margins so that the extent for these three sectors is relatively confident.

6.2. Overall tendency of changes

The Hailuogou Glacier was in rapid recession during the study period. The glacier surface elevation lowered consistently between 2018 and 2021, and the glacier terminus retreated more than 350 m (Figure 7(B)). The overall area of the glacier tongue also reduced year on year (Figure 7(C)). Except for the lower part of the ice tongue, the spatial distribution of both crevasses and ice cliffs did not change significantly in Sectors 2, 3 and 4, with all three showing a slight decline in their key statistics (Figure 7(C,D)). The main changes in crevasse and ice cliff characteristics are mainly observed near the end of the glacier terminus. The changes observed around the glacier terminus were mainly controlled by the combination of melting and ice collapsing (Xu et al., 2022). As evident by the statistical analysis of crevasses density (Figure 7(C)), the glacier terminus (Sector 1) has become more crevassed. Due to intensified ablation and subsequent
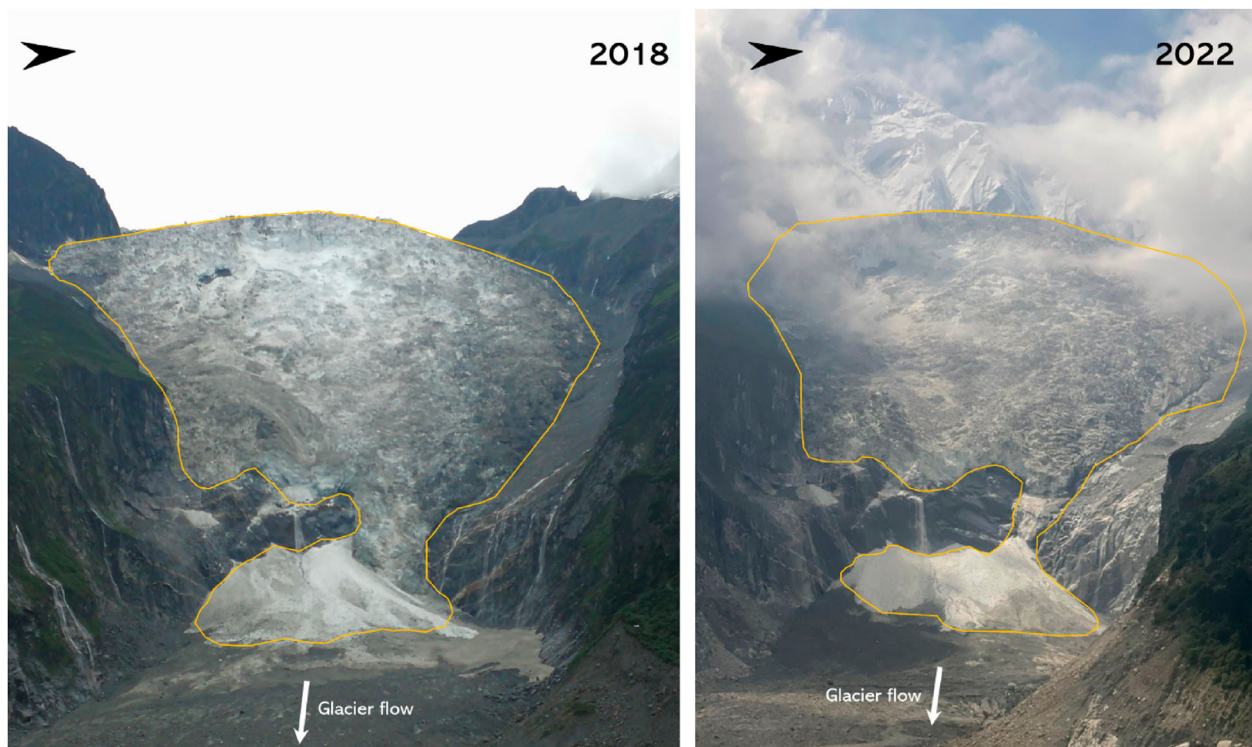

Figure 8. A comparison of Hailuogou Glacier icefall between 2018 and 2022.

ice collapse events around the outlet of the subglacial river, the frontal ice margin is now arcuate, and ice debris and fresh ice were frequently found around the collapsed frontal cliffs at the glacier terminus.

6.3. Mechanism of interannual glacier changes and implications

Interannual comparisons have revealed similar behavior through time relating to glacier dynamics and its rapid evolution. The most significant evidence for supporting that the glacier was in a heavy recession is the remarkable increase we record in crevasse density and cliff density for Sector 1, as well as the areal shrinkage and the systematic lowering of the ice surface profiles. Specifically, the increase in crevasse density for Sector 1 (i.e. 8.43–38.59 km/km^2) verified that the lower glacier tongue is in the process of progressive disintegration, with frequent frontal ice collapse particularly focusing around the subglacial portal (Xu et al., 2022).

By the end of 2021, the ice fall of Hailuogou Glacier had become nearly disconnected with the accumulation area (Figure 8). Continuous thinning and narrowing of the ice fall reduces the mass flux transferred down-glacier, impacting heavily on the lower part of the glacier (Zhang et al., 2010; Zhong et al., 2022). Coincident with this reduction in mass from higher elevation is the onset of rapid terminus recession through ice collapse and its broader disintegration. The lower tongue is therefore being simultaneously starved of mass at its upper end, and eroded by hydrological processes at its lower end, a scenario which is not common for ablation of valley glaciers. The ring-shape cracks on the glacier surface have a strong relationship with the roof collapse of the englacial or subglacial conduits (Egli et al., 2021). Considerable areas of ice debris falling from the glacier terminus also indicate the unstable condition of the glacier snout. The number of glaciological features evident on the 2021 map is far fewer than in the earlier three years, suggesting that the glacier is becoming increasingly stagnant, and tending towards becoming dead ice due to its disconnection with the accumulation zone.

7. Conclusions

We mapped a variety of features for the Hailuogou Glacier tongue based on clearly defined mapping criteria. The key features included glaciological, glacial geomorphological and hydrological features. Based on the mapping results and analyzes, we assessed the evolution of the Hailuogou Glacier tongue during 2018–2021. We interpret these features to illustrate that the glacier is in rapid recession, and even possibly disintegration. The disconnection between the glacier tongue and the accumulation zone has set the lower part of the glacier on a course to becoming stagnant, and ultimately existing only as a block of dead ice.

Therefore, it can be hypothesized that the glacier will only recede more rapidly over the next decades, with the exact rate being determined largely by the magnitude-frequency of future terminus ice collapse events.

Software

All aerial images were imported into Agisoft Metashape Pro v1.5.3 for processing. All mapping and digitizing works were conducted by ESRI ArcGIS 10.3.

Data availability statement

The data that support the findings of this study are available from the corresponding author, Ping Fu, upon reasonable request.

References

Azzoni, R. S., Fugazza, D., Zennaro, M., Zucali, M., D'Agata, C., Maragno, D., Cernuschi, M., Smiraglia, C., & Diolaiuti, G. A. (2017). Recent structural evolution of forni glacier tongue (ortles-cevedale group, central Italian Alps). *Journal of Maps*, *13*(2), 870–878. https://doi.org/10.1080/17445647.2017.1394227

Bash, E. A., Moorman, B. J., & Gunther, A. (2018). Detecting short-term surface melt on an Arctic glacier using UAV surveys. *Remote Sensing*, *10*(10), 1547. https://doi.org/10.3390/rs10101547

Benn, D. I., & Evans, D. J. A. (2013). *Glaciers & glaciation* (2nd ed). Routledge.

Benn, D. I., Thompson, S., Gulley, J., Mertes, J., Luckman, A., & Nicholson, L. (2017). Structure and evolution of the drainage system of a Himalayan debris-covered glacier, and its relationship with patterns of mass loss. *The Cryosphere*, *11*(5), 2247–2264. https://doi.org/10.5194/tc-11-2247-2017

Chandler, B. M. P., Lovell, H., Boston, C. M., Lukas, S., Barr, I. D., Benediktsson, ÍÖ, Benn, D. I., Clark, C. D., Darvill, C. M., Evans, D. J. A., Ewertowski, M. W., Loibl, D., Margold, M., Otto, J.-C., Roberts, D. H., Stokes, C. R., Storrar, R. D., & Stroeven, A. P. (2018). Glacial geomorphological mapping: A review of approaches and frameworks for best practice. *Earth-Science Reviews*, *185*, 806–846. https://doi.org/10.1016/j.earscirev.2018.07.015

Chudley, T. R., Christoffersen, P., Doyle, S. H., Abellan, A., & Snooke, N. (2019). High-accuracy UAV photogrammetry of ice sheet dynamics with no ground control. *The Cryosphere*, 13(3), 955–968. https://doi.org/10.5194/tc-13-955-2019

Colgan, W., Rajaram, H., Abdalati, W., McCutchan, C., Mottram, R., Moussavi, M. S., & Grigsby, S. (2016). Glacier crevasses: Observations, models, and mass balance implications. *Reviews of Geophysics*, 54(1), 119–161. https://doi.org/10.1002/2015RG000504

Darnault, R., Rolland, Y., Braucher, R., Bourlès, D., Revel, M., Sanchez, G., & Bouissou, S. (2012). Timing of the last deglaciation revealed by receding glaciers at the Alpine-scale: impact on mountain geomorphology. *Quaternary Science Reviews*, 31, 127–142. https://doi.org/10.1016/j.quascirev.2011.10.019

Egli, P. E., Belotti, B., Ouvry, B., Irving, J., & Lane, S. N. (2021). Subglacial channels, climate warming, and increasing frequency of alpine glacier snout collapse. *Geophysical Research Letters*, 48, e2021GL096031. https://doi.org/10.1029/2021GL096031

Forlani, G., Dall'Asta, E., Diotri, F., Cella, U. M. d., Roncella, R., & Santise, M. (2018). Quality assessment of DSMs produced from UAV flights georeferenced with On-board RTK positioning. *Remote Sensing*, 10(2), 311. https://doi.org/10.3390/rs10020311

Fu, P., Harbor, J. M., Stroeven, A. P., Hättestrand, C., Heyman, J., & Zhou, L. (2013). Glacial geomorphology and paleoglaciation patterns in Shaluli Shan, the southeastern Tibetan Plateau — Evidence for polythermal ice cap glaciation. *Geomorphology*, 182, 66–78. https://doi.org/10.1016/j.geomorph.2012.10.030

Fu, P., Heyman, J., Hättestrand, C., Stroeven, A. P., & Harbor, J. M. (2012). Glacial geomorphology of the shaluli shan area, southeastern Tibetan plateau. *Journal of Maps*, 8, 48–55. https://doi.org/10.1080/17445647.2012.668762

Gindraux, S., Boesch, R., & Farinotti, D. (2017). Accuracy assessment of digital surface models from unmanned aerial vehicles' imagery on glaciers. *Remote Sensing*, 9(2), 186. https://doi.org/10.3390/rs9020186

Goodsell, B., Hambrey, M. J., Glasser, N. F., Nienow, P., & Mair, D. (2005). The structural glaciology of a temperate valley glacier: Haut glacier D'Arolla, Valais, Switzerland. *Arctic, Antarctic, and Alpine Research*, 37(2), 218–232. https://doi.org/10.1657/1523-0430(2005)037[0218:TSGOAT]2.0.CO;2

Guo, W., Liu, S., Xu, J., Wu, L., Shangguan, D., Yao, X., Wei, J., Bao, W., Yu, P., Liu, Q., & Jiang, Z. (2015). The second Chinese glacier inventory: data, methods and results. *Journal of Glaciology*, 61(226), 357–372. https://doi.org/10.3189/2015JoG14J209

Heim, A. (1936). The glaciation and solifluction of minya gongkar. *The Geographical Journal*, 87(5), 444–450. https://doi.org/10.2307/1785645

Huang, M., Wang, M., Song, G., Li, G., & Shen, Y. (1996). Hydraulic effecrs in the ablation area of the hailuogou glacier. *Journal of Glaciology and Geocryology*, 18, 46–50.

IPCC. (2021). Summary for Policymakers. In: *Climate Change 2021: The Physical Science Basis. Contribution of Working Group I to the Sixth Assessment Report of the Intergovernmental Panel on Climate Change* (pp. 3–32). Cambridge, UK and New York, NY, USA: Cambridge University Press. https://doi.org/10.1017/9781009157896.001

Jennings, S. J. A., & Hambrey, M. J. (2021). Structures and deformation in glaciers and Ice sheets. *Reviews of Geophysics*, 59(3), e2021RG000743. https://doi.org/10.1029/2021RG000743

Jennings, S. J. A., Hambrey, M. J., Glasser, N. F., James, T. D., & Hubbard, B. (2016). Structural glaciology of Austre Brøggerbreen, Northwest Svalbard. *Journal of Maps*, 12, 790–796. https://doi.org/10.1080/17445647.2015.1076744

Jones, C., Ryan, J., Holt, T., & Hubbard, A. (2018). Structural glaciology of isunguata sermia, west Greenland. *Journal of Maps*, 14, 517–527. https://doi.org/10.1080/17445647.2018.1507952

Jouberton, A., Shaw, T. E., Miles, E., McCarthy, M., Fugger, S., Ren, S., Dehecq, A., Yang, W., & Pellicciotti, F. (2022). Warming-induced monsoon precipitation phase change intensifies glacier mass loss in the southeastern Tibetan Plateau. *Proceedings of the National Academy of Sciences*, 119, e2109796119. https://doi.org/10.1073/pnas.2109796119

Kirkbride, M. P. (1993). The temporal significance of transitions from melting to calving termini at glaciers in the central Southern Alps of New Zealand. *The Holocene*, 3(3), 232–240. https://doi.org/10.1177/095968369300300305

Kirkbride, M. P., & Warren, C. R. (1999). Tasman Glacier, New Zealand: 20th-century thinning and predicted calving retreat. *Global and Planetary Change*, 22(1-4), 11–28. https://doi.org/10.1016/S0921-8181(99)00021-1

Kneib, M., Miles, E. S., Jola, S., Buri, P., Herreid, S., Bhattacharya, A., Watson, C. S., Bolch, T., Quincey, D., & Pellicciotti, F. (2021). Mapping ice cliffs on debris-covered glaciers using multispectral satellite images. *Remote Sensing of Environment*, 253, 112201. https://doi.org/10.1016/j.rse.2020.112201

Lardeux, P., Glasser, N., Holt, T., & Hubbard, B. (2016). Glaciological and geomorphological map of glacier noir and glacier blanc, French Alps. *Journal of Maps*, 12, 582–596. https://doi.org/10.1080/17445647.2015.1054905

Li, Y., & Fu, P. (2019). Mapping the late-holocene glacial geomorphology and glacier surface types in the Mt. Harajoriha, central Tian Shan. *International Journal of Geosciences*, 10(6), 669–688. https://doi.org/10.4236/ijg.2019.106038

Li, Z., He, Y., Yang, X., Theakstone, W. H., Jia, W., Pu, T., Liu, Q., He, X., Song, B., Zhang, N., Wang, S., & Du, J. (2010). Changes of the Hailuogou glacier, Mt. Gongga, China, against the background of climate change during the Holocene. *Quaternary International*, 218(1-2), 166–175. https://doi.org/10.1016/j.quaint.2008.09.005

Liao, H., Liu, Q., Zhong, Y., & Lu, X. (2020). Landsat-Based estimation of the glacier surface temperature of hailuogou glacier, southeastern Tibetan plateau, between 1990 and 2018. *Remote Sensing*, 12(13), 2105. https://doi.org/10.3390/rs12132105

Liu, Q., & Liu, S. (2010). Seasonal evolution of the englacial and subglacial drainage systems of a temperate glacier revealed by hydrological analysis. *Sciences in Cold and Arid Regions*, 2, 51–58.

Liu, Q., Liu, S., & Cao, W. (2018). Seasonal variation of drainage system in the lower ablation area of a monsoonal temperate debris-covered glacier in Mt. Gongga, southeastern tibet. *Water*, 10, 1050. https://doi.org/10.3390/w10081050

Liu, Q., Liu, S., Zhang, Y., Wang, X., Zhang, Y., Guo, W., & Xu, J. (2010). Recent shrinkage and hydrological response of Hailuogou glacier, a monsoon temperate glacier on the east slope of Mount Gongga, China. *Journal of Glaciology*, 56(196), 215–224. https://doi.org/10.3189/002214310791968520

Lu, R., & Gao, S. (1992). Debris flow in the Ice tongue area of hailuogou glacier on the eastern slope of Mt.gongga. *Journal of Glaciology and Geocryology*, 14, 73–80.

Mallalieu, J., Carrivick, J. L., Quincey, D. J., Smith, M. W., & James, W. H. M. (2017). An integrated Structure-from-Motion and time-lapse technique for quantifying ice-margin dynamics. *Journal of Glaciology*, 63(242), 937–949. https://doi.org/10.1017/jog.2017.48

Miles, E. S., Steiner, J., Willis, I., Buri, P., Immerzeel, W. W., Chesnokova, A., & Pellicciotti, F. (2017). Pond dynamics and supraglacial-englacial connectivity on debris-covered lirung glacier, Nepal. *Frontiers in Earth Science*, 5, 69. https://doi.org/10.3389/feart.2017.00069

Owen, L. A., Caffee, M. W., Finkel, R. C., & Seong, Y. B. (2008). Quaternary glaciation of the Himalayan–Tibetan orogen. *Journal of Quaternary Science*, 23(6-7), 513–531. https://doi.org/10.1002/jqs.1203

Rossini, M., Di Mauro, B., Garzonio, R., Baccolo, G., Cavallini, G., Mattavelli, M., De Amicis, M., & Colombo, R. (2018). Rapid melting dynamics of an alpine glacier with repeated UAV photogrammetry. *Geomorphology*, 304, 159–172. https://doi.org/10.1016/j.geomorph.2017.12.039

Sakai, A., Nakawo, M., & Fujita, K. (2002). Distribution characteristics and energy balance of Ice cliffs on debris-covered glaciers, Nepal himalaya. *Arctic, Antarctic, and Alpine Research*, 34(1), 12–19. https://doi.org/10.1080/15230430.2002.12003463

Sakai, A., Nishimura, K., Kadota, T., & Takeuchi, N. (2009). Onset of calving at supraglacial lakes on debris-covered glaciers of the Nepal Himalaya. *Journal of Glaciology*, 55(193), 909–917. https://doi.org/10.3189/002214309790152555

Smith, M. W., Carrivick, J. L., & Quincey, D. J. (2016). Structure from motion photogrammetry in physical geography. *Progress in Physical Geography: Earth and Environment*, 40(2), 247–275. https://doi.org/10.1177/0309133315615805

Su, Z., Song, G., & Cao, Z. (1996). Maritime characteristics of hailuogou glacier in the gongga mountain. *Journal of Glaciology and Geocryology*, 18, 51–59.

Tadono, T., Nagai, H., Ishida, H., Oda, F., Naito, S., Minakawa, K., & Iwamoto, H. (2016). Generation of the 30 M-mesh global digital surface model by alos prism. *The International Archives of the Photogrammetry, Remote Sensing and Spatial Information Sciences*, 41B4, 157–162. https://doi.org/10.5194/isprs-archives-XLI-B4-157-2016

Usgs. (1997). *30 ARC-second global elevation data, GTOPO30, research data archive at the national center for atmospheric research*. Computational and Information Systems Laboratory. https://doi.org/10.5065/A1Z4-EE71.

Vaughan, D. G. (1993). Relating the occurrence of crevasses to surface strain rates. *Journal of Glaciology*, 39(132), 255–266. https://doi.org/10.1017/S0022143000015926

Villanueva, J. K. S., & Blanco, A. C. (2019). Optimization of ground control point (GCP) configuration for unmanned aerial vehicle (UAV) survey using structure from motion (SFM). *The International Archives of the Photogrammetry, Remote Sensing and Spatial Information Sciences*, XLII-4/W12, 167–174. https://doi.org/10.5194/isprs-archives-XLII-4-W12-167-2019

Wang, S., Che, Y., & Wei, Y. (2021). Spatiotemporal dynamic characteristics of typical temperate glaciers in China. *Scientific Reports*, 11(1), 657. https://doi.org/10.1038/s41598-020-80418-7

Watson, C. S., Quincey, D. J., Carrivick, J. L., & Smith, M. W. (2016). The dynamics of supraglacial ponds in the Everest region, central Himalaya. *Global and Planetary Change*, 142, 14–27. https://doi.org/10.1016/j.gloplacha.2016.04.008

Watson, C. S., Quincey, D. J., Smith, M. W., Carrivick, J. L., Rowan, A. V., & James, M. R. (2017). Quantifying ice cliff evolution with multi-temporal point clouds on the debris-covered Khumbu Glacier, Nepal. *Journal of Glaciology*, 63(241), 823–837. https://doi.org/10.1017/jog.2017.47

Xu, S., Fu, P., Quincey, D., Feng, M., Marsh, S., & Liu, Q. (2022). UAV-based geomorphological evolution of the terminus area of the hailuogou glacier, southeastern Tibetan plateau between 2017 and 2020. *Geomorphology*, 411, 108293. https://doi.org/10.1016/j.geomorph.2022.108293

Yang, K., & Liu, Q. (2016). Supraglacial drainage system: a review. *Journal of Glaciology and Geocryology*, 38, 1666–1678.

Yang, W., Yao, T., Guo, X., Zhu, M., Li, S., & Kattel, D. B. (2013). Mass balance of a maritime glacier on the southeast Tibetan Plateau and its climatic sensitivity. *Journal of Geophysical Research: Atmospheres*, 118(17), 9579–9594. https://doi.org/10.1002/jgrd.50760

Zemp, M., Frey, H., Gärtner-Roer, I., Nussbaumer, S. U., Hoelzle, M., Paul, F., Haeberli, W., Denzinger, F., Ahlstrøm, A. P., Anderson, B., Bajracharya, S., Baroni, C., Braun, L. N., Cáceres, B. E., Casassa, G., Cobos, G., Dávila, L. R., Granados, H. D., Demuth, M. N., … Vincent, C. (2015). Historically unprecedented global glacier decline in the early 21st century. *Journal of Glaciology*, 61(228), 745–762. https://doi.org/10.3189/2015JoG15J017

Zhang, Y., Fujita, K., Liu, S., Liu, Q., & Nuimura, T. (2011). Distribution of debris thickness and its effect on ice melt at Hailuogou glacier, southeastern Tibetan Plateau, using in situ surveys and ASTER imagery. *Journal of Glaciology*, 57(206), 1147–1157. https://doi.org/10.3189/002214311798843331

Zhang, Y., Fujita, K., Liu, S., Liu, Q., & Wang, X. (2010). Multi-decadal ice-velocity and elevation changes of a monsoonal maritime glacier: Hailuogou glacier, China. *Journal of Glaciology*, 56(195), 65–74. https://doi.org/10.3189/002214310791190884

Zhang, Y., Hirabayashi, Y., & Liu, S. (2012). Catchment-scale reconstruction of glacier mass balance using observations and global climate data: Case study of the Hailuogou catchment, south-eastern Tibetan Plateau. *Journal of Hydrology*, 444-445, 146–160. https://doi.org/10.1016/j.jhydrol.2012.04.014

Zhang, Y., Liu, S., Liu, Q., Wang, X., Jiang, Z., & Wei, J. (2019). The role of debris cover in catchment runoff: A case study of the hailuogou catchment, south-eastern Tibetan plateau. *Water*, 11(12), 2601. https://doi.org/10.3390/w11122601

Zhong, Y., Liu, Q., Westoby, M., Nie, Y., Pellicciotti, F., Zhang, B., Cai, J., Liu, G., Liao, H., & Lu, X. (2022). Intensified paraglacial slope failures due to accelerating downwasting of a temperate glacier in Mt. Gongga, southeastern Tibetan Plateau. *Earth Surface Dynamics*, 10(1), 23–42. https://doi.org/10.5194/esurf-10-23-2022